Bio-Design and Manufacturing (2021) 4:806–817
https://doi.org/10.1007/s42242-021-00138-3

RESEARCH ARTICLE

Evaluation of a resorufin-based fluorescent probe for tyrosinase detection in skin pigmentation disorders

Yibo Hu[1] · Hongliang Zeng[2] · Jiaxing Jiang[3] · Sheng Yang[3] · Jinhua Huang[1] · Jing Chen[1] · Qinghai Zeng[1]

Received: 15 January 2021 / Accepted: 27 May 2021 / Published online: 21 July 2021

Abstract

Purpose Skin pigmentation disorders, such as vitiligo and melasma, are difficult to diagnose in the early stages, but abnormal tyrosinase levels and tyrosinase activity are potential indicators. Some resorufin-based fluorescence probes (RBFPs) have been designed to detect tyrosinase in tumors, but they have not been used in skin pigmentation disorders. In this study, one of these RBFPs (synthesized by resorufin salt coupled with 3-(bromomethyl)phenol) was evaluated comprehensively.

Methods The RBFP was tested in different kinds of mouse and human skin cells, as well as in in vivo models, including zebrafish, guinea pigs, and Sprague–Dawley rats. In addition, small interfering RNAs (siRNAs), kojic acid, and 1-phenyl-2-thiourea (PTU) were used to inhibit tyrosinase levels or tyrosinase activity.

Results This probe successfully detected tyrosinase and emitted red fluorescence in melanoma cells and melanocytes. Fluorescence was also observable in zebrafish and on the skin of guinea pigs when using the RBFP. In mouse and human cells, the RBFP showed good selectivity to tyrosinase. Moreover, in the case of decreased tyrosinase levels or activity caused by siRNAs, kojic acid, or PTU, the probe was sensitive to these changes. Further, the RBFP showed no toxic effects at concentrations of < 20 μmol/L, both in vitro and in vivo.

Conclusions Our findings indicate the value and limitations of the RBFP in tyrosinase detection, but suggest the need for further improvement of fluorescent probes in the diagnosis of skin pigmentation disorders.

Jing Chen and Qinghai Zeng contributed equally to this work.

✉ Jing Chen
43700351@qq.com

✉ Qinghai Zeng
zengqinghai@csu.edu.cn

[1] Department of Dermatology, The Third Xiangya Hospital of Central South University, Tongzipo Road No.138, Yuelu District, Changsha 410013, China

[2] Institute of Chinese Materia Medica, Hunan Academy of Chinese Medicine, Changsha 410006, China

[3] School of Chemistry and Food Engineering, Changsha University of Science and Technology (CSUST), Changsha 410114, China

Graphic abstract

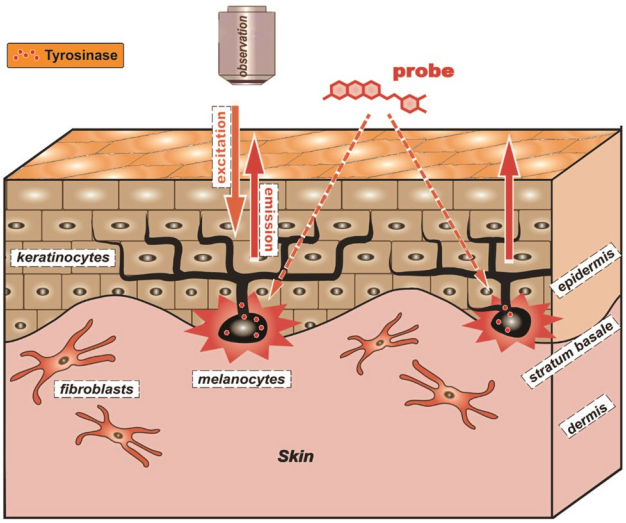

Keywords Tyrosinase · Pigmentation disorder · Diagnosis · Fluorescence probe

Background

Skin pigmentation disorders, such as vitiligo, melasma, freckles, and achromic nevus, are common afflictions that can affect the mental health and social life of people with these disorders [1–4]. Tyrosinase (TYR) is the key enzyme that catalyzes the copper-based oxidation of phenols and chromophore production [5]. Thus, TYR plays a critical role in pigmentation by catalyzing L-tyrosine to L-3,4-dihydroxyphenylalanine (L-DOPA) and further converting L-DOPA to dopaquinone and melanin [6–8]. Abnormal TYR levels or activity is important feature of pigmentation disorders. For example, the main pathogenic changes in vitiligo are melanocyte loss and TYR dysfunction, which may be caused by oxidative stress, inflammation, and autoimmunity [9, 10]. The main biochemical feature of melasma and freckles is the overproduction of melanin [11, 12]; many reagents have been developed to tackle excessive TYR [13].

Early diagnosis is essential to treat pigmentation disorders [2, 14–16]. In clinical practice, diagnosis of vitiligo and melasma depends mainly on skin appearance and uses Wood's lamp ultraviolet tests and skin reflectance confocal microscopy (RCM) to facilitate detection and examination of lesions [17–19]. Visual detection of anomalies is still difficult in the early stages that lack obvious lesions. However, changes in TYR expression or activity in melanocytes already exist at these early stages [20, 21], suggesting that TYR could be an ideal marker for early diagnosis. Several assays have been developed to detect human serum TYR that show promise as tools for clinical diagnosis [22]. However, there is no widely accepted diagnostic method for detecting TYR in skin.

Recently, researchers have designed specific fluorescent probes to detect TYR in tumor cells, some of which are resorufin-based fluorescence probes (RBFPs). RBFPs can be selectively hydroxylated by TYR in B16, HepG2, MCF-7 cells, and zebrafish [23–25], suggesting the potential value of RBFPs for use in complex biosystems. However, there has been no research to investigate whether RBFPs also work for diagnosis of other TYR-related diseases, such as skin pigmentation disorders. Thus, we studied one of the reported RBFPs (synthesized by resorufin salt coupled with 3-(bromomethyl)phenol, the synthesis and reaction mechanism diagram are shown in Fig. 1a) for possible use as a skin-disorder indicator in skin. Different types of skin cells and in vivo models were tested to comprehensively assess the performance of the RBFP. In addition, small interfering RNAs (siRNAs), kojic acid, and 1-phenyl-2-thiourea (PTU) were used as reagents to induce abnormal TYR expression and activity. Our investigation aims to confirm the potential value and limitations of RBFPs in skin pigmentation disorders.

Materials and methods

Reagents and cell culture medium

Chemical reagents were obtained from commercial suppliers. siRNAs were supplied by GenePharma (Shanghai,

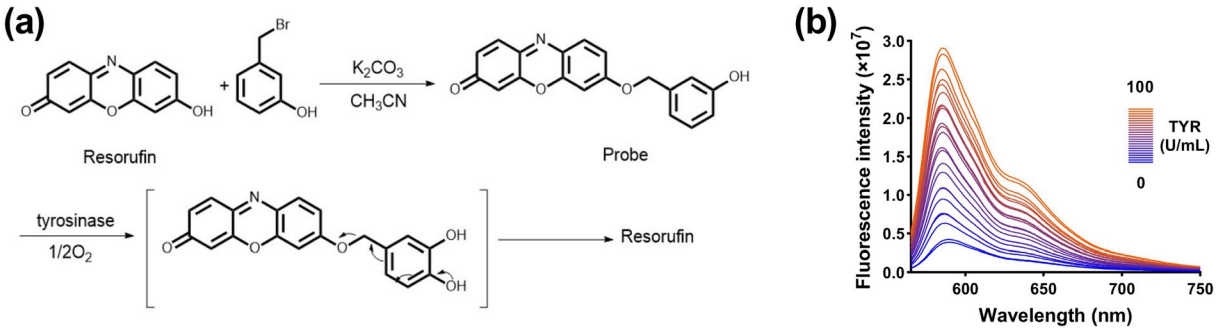

Fig. 1 Mechanism and performance of the RBFP in tyrosinase (TYR) detection: **a** The synthesis and reaction mechanism of the RBFP; **b** The titration curve shows the emission spectra of the RBFP (5 μmol/L) in the presence of various TYR concentrations (0–100 U/mL)

China). Kojic acid was supplied by Solarbio Science & Technology (Beijing, China). PTU was supplied by Seebio Biotech (Shanghai, China). 3-(4,5-Dimethylthiazol-2-yl)-2,5-diphenyltetrazolium bromide (MTT) and dithiothreitol (DTT) were supplied by Sigma-Aldrich (Shanghai, China). Phorbol 12-myristate 13-acetate (PMA) was supplied by MutiSciences (Hangzhou, China). Fetal bovine serum (FBS) was supplied by Biological Industries (Beit-Haemek, Israel). Human melanocyte growth supplement (HMGS), 254 medium, and Dulbecco's modified Eagle medium (DMEM) were supplied by Gibco (Gaithersburg, MD, USA). Keratinocyte growth medium (KGM) was supplied by PromoCell (Heidelberg, Germany).

Probe synthesis

Scheme S1 depicts the synthetic procedure of the RBFP used in this study. *m*-(hydroxy benzyl) alcohol (compound 1) was first treated with phosphorus tribromide to give 3-(bromomethyl) phenol (compound 2); compound 2 and resorufin were then covalently linked to give the final probe molecule. Details for synthesis and characterization of this RBFP are described in the supplementary materials [25]. After synthesized, the RBFP was dissolved in DMSO and stored at 20 mmol/L, and the final concentration of DMSO was 0.1% when diluted RBFP to 20 μmol/L.

Spectrophotometric experiments

To confirm the selectivity of the probe for tyrosinase, test solutions were prepared by mixing RBFP (the final concentration is 5 μmol/L) and appropriate analyte stock (potential interfering species, the details of them are shown in Fig. S2) into a tube separately and then diluting the solution to 500 μL with 67 mmol/L phosphate-buffered saline (PBS; pH 7.4). After incubation at 37 °C for 3 h, the absorption or fluorescence spectra were then determined under a fluorescence microscope. The fluorescence spectra were recorded at emission wavelengths ranging from 565 to 750 nm with excitation at 550 nm.

Cell culturing

The murine melanoma cell line B16F10 was obtained from the China Center for Type Culture Collection (CCTCC). Murine melanocyte Melan-a was a kind gift from Prof. Dorothy C. Bennett (St. George's Hospital, London, UK) and given by Renmin Hospital of Wuhan University (Wuhan, China), cultured in RPMI-1640 medium with 10% FBS, 100 μmol/L DTT, and 200 nmol/L PMA. The human melanoma cell line MNT1 was from Dr. Vince Hearing (Pigment Cell Biology Section, NCI, NIH, USA) and generously provided by Renmin Hospital of Wuhan University. Human immortalized melanocytes (PIG1) was a gift from Dr. Caroline Le Poole (Loyola University, Chicago, USA). Human skin immortalized keratinocytes (HaCaT) were obtained from the American Center for Type Culture Collection (ATCC). Primary human epidermal melanocytes (HEMs), keratinocytes, and fibroblasts were separated from volunteers' foreskin (approved by donors and the Ethics Committee of the Third Xiangya Hospital, Central South University, Changsha, China), using a protocol described previously [26]. PIG1 and HEMs were cultured in 254 medium with 1% HMGS and 5% FBS, and keratinocytes were cultured in serum-free KGM. B16F10, HaCaT cells, and fibroblasts were cultured in DMEM with 10% FBS and 1% penicillin–streptomycin solution added to the medium. All cells were cultured in a 5% CO_2 incubator at 37 °C. Cell morphology and fluorescence were observed using an inverted fluorescence microscope (Olympus, Japan), with excitation at approximately (546 ± 10) nm, and emission around (595 ± 60) nm.

Cell viability assay

Cell viability was measured using an MTT assay. Cells (3000–5000) were added into each well of a 96-well plate,

with a control group to which only medium was added. Cells were attached to the wells after 8–12 h, then treated with RBFP at different concentrations (0, 0.3, 0.6, 1.2, 2.5, 5.0, 10.0, and 20.0 μmol/L) for 12, 24, 36, and 48 h. Before measurement, 20 μL MTT was added into each well and the cells were incubated at 37 °C for 4 h. We then removed all the medium carefully, added 160 μL dimethyl sulfoxide (DMSO), and incubated the plate at 37 °C for 15 min away from light. The absorbance value at 490 nm was measured by a microplate reader (PerkinElmer, USA).

RNA interfering

Cells were added to six-well plates and transfected at a confluence of 60%. siRNAs were diluted with DNase/RNase-free water to 20 μmol/L; next, 10 μL of the siRNA solution and 10 μL HiperFect transfection reagent (QIAGEN, Germany) were mixed with basal cell culture medium and incubated for 5–10 min. The mixture was then added to the cells and knockdown efficiency was measured by quantitative real-time reverse transcriptional polymerase chain reaction (qRT-PCR) 48 h later.

RNA extraction and qRT-PCR

Cells were collected in tubes after digestion by trypsin; the cell pellets were then washed twice with PBS and lysed with 1 mL Trizol lysis buffer. Total RNA was extracted with Total RNA Kit (Omega, USA) and reversely transcripted with ReverTra Ace qPCR RT Master Mix Kit (Toyobo, Japan). qRT-PCR was conducted with a KOD SYBR® qPCR Kit (Toyobo, Japan); the amplification followed the three-step method in a cycler (Roche, Switzerland). The sequences of primer pairs used in amplification are provided in Table S1.

Zebrafish culture

Zebrafish embryos and special zebrafish culture medium were supplied by EzeRinka (Nanjing, China). The embryos were cultured and hatched at 24 °C away from light. Then, the fish were incubated with 200 μmol/L PTU or medium only; the RBFP was added 24 h before observation. A fluorescence microscope was used to observe the fluorescence at (595 ± 60) nm, as well as the distribution and density of melanin granules.

Guinea pig and Sprague–Dawley rat experiment

Female Guinea pigs (Dunkin Hartley) were supplied by Taiping Biotech (Hunan, China), Sprague–Dawley (SD) rats (*Rattus norvegicus*) were supplied by SJA Laboratory Animal Co., Ltd (Hunan, China). The experiment was approved by the Animal Welfare Committee of the Department of Laboratory Animals, Central South University, Changsha, China. The dorsal skin of guinea pigs was shaved and divided into four quadrants, then coated with kojic acid solution or PBS. The RBFP was added 4 h before observation and the fluorescence was detected with an in vivo imaging system (PerkinElmer, USA). SD rats were treated with RBFP (20 μmol/L) twice a day for 3 d. The appearance of the skin was observed and organs were collected after experiment. Samples were fixed with 4% paraformaldehyde and stained with hematoxylin–eosin (HE).

Statistical analysis

All experiments were repeated independently at least three times. Data were analyzed by Student's *t*-tests or one-way analysis of variance (ANOVA). The data are shown graphically by GraphPad Prism (Version 8.0, GraphPad Software, San Diego, USA) and expressed as mean ± standard deviation. $P < 0.05$ was considered statistically significant and identified with an asterisk ($^{*}P < 0.05$, $^{**}P < 0.01$).

Results

Mechanism of the RBFP in vitro

First, we evaluated the performance of the RBFP in detection of TYR. Without TYR, the RBFP (5 μmol/L) displayed only weak fluorescence, which peaked at 586 nm; however, the addition of increasing concentrations of TYR to the aqueous solution of RBFP at pH 7.4 elicited dramatic enhancement of the emission spectra (Fig. 1b). There was a strong linear correlation between fluorescence intensity and TYR concentrations 0 to 100 U/mL (Fig. S1).

A bioimaging probe with high specificity to the target molecule over other potentially competing is of great importance in complex biosystems. Therefore, evaluation of the selectivity of the RBFP was tested with various biologically relevant molecules including metal ions, reactive oxygen species (ROS), reducing agents, small molecule thiols, and other enzymes (The selectivity of the RBFP to different molecules was tested separately). As shown in Fig. S2, apart from TYR, no obvious variations in fluorescence were observed in the presence of these interfering species. Moreover, the RBFP was stable and could respond to TYR at biologically relevant pH levels (Fig. S3).

Cytotoxicity of the RBFP

In mice and humans, both melanoma cells and melanocytes share similarities in melanin production [27, 28]. Thus,

we used four types of cell models for in vitro experiments, including two mouse-cell models [mouse melanoma cell line B16F10 and mouse melanocyte cell line (Melan-a)] and two human models [human melanoma cell line MNT1 and primary epidermal melanocytes (HEMs)]. To determine the cytotoxicity of RBFP, we determined the viability of B16F10, Melan-a, MNT1, and HEMs using an MTT assay. The cells were treated with different concentrations of RBFP ranging from 0 to 20 μmol/L, and absorbance at 490 nm was measured 12, 24, 36, and 48 h after treatment.

In mouse B16F10 and Melan-a cells, the RBFP showed no impact on cell viability at concentrations lower than 20 μmol/L, but cell viability decreased significantly in the 20 μmol/L group ($P < 0.05$, Fig. 2a and 2b). Besides, viability of human MNT1 cells was not affected by RBFP treatment. HEMs, however, showed a different result. When RBFP concentrations reached 20 μmol/L, HEM viability decreased significantly at 12, 24, 36, and 48 h ($P < 0.05$, shown in Fig. 2c and 2d).

Performance of the RBFP in different skin cells

Although this RBFP had been found to have good selectivity for TYR in our in vitro experiments, its selectivity has not been evaluated in different kinds of skin cells. Thus, we also tested this RBFP in human melanocyte cell line PIG1, human keratinocyte cell line HaCaT, human primary skin fibroblasts (FB), keratinocytes (KC), and HEMs. In PIG1, HaCaT, and FB, only weak fluorescence was observed after RBFP treatment (Fig. 3a). In addition, in co-cultured HEMs and KC, HEMs showed strong fluorescence, but KC showed only weak red fluorescence (Fig. 3b), and that HEMs were therefore easy to distinguish from KC. qRT-PCR results showed that the RNA levels of TYR in HEMs and PIG1 cells were much higher than those in HaCaT, FB, and KC cells (Fig. 3c).

Observation conditions and clearance of the RBFP in cells

We further investigated the optimal concentration and treating time of the RBFP in TYR detection. First, B16F10 cells were treated with the RBFP at different concentrations (2.5, 5.0, and 10.0 μmol/L), and cell fluorescence was observed at several time points (8, 16, 24, and 36 h); fresh probe was added after each observation. Under a fluorescence microscope, red fluorescence was enhanced as RBFP concentration and incubation time increased (Fig. 4a). In the 5.0 and 10.0 μmol/L groups, fluorescence was visible at 8 h and became stronger at 16 h. However, the 2.5 μmol/L group showed only weak fluorescence. After 36 h of treatment, the fluorescence intensity was increased in all groups.

We also used MNT1 and HEMs to verify the performance of the RBFP after 24 h of treatment, at different probe concentrations (0–20 μmol/L). After treatment, we removed the RBFP and observed clearance of intracellular RBFP. At 24 h, MNT1 and HEMs only showed weak fluorescence under 1 μmol/L RBFP treatment, but fluorescence intensity gradually increased with increased concentration, similar to results of RBFP treated B16F10 cells. After the RBFP was removed, fluorescence was still visible in MNT1 and HEMs

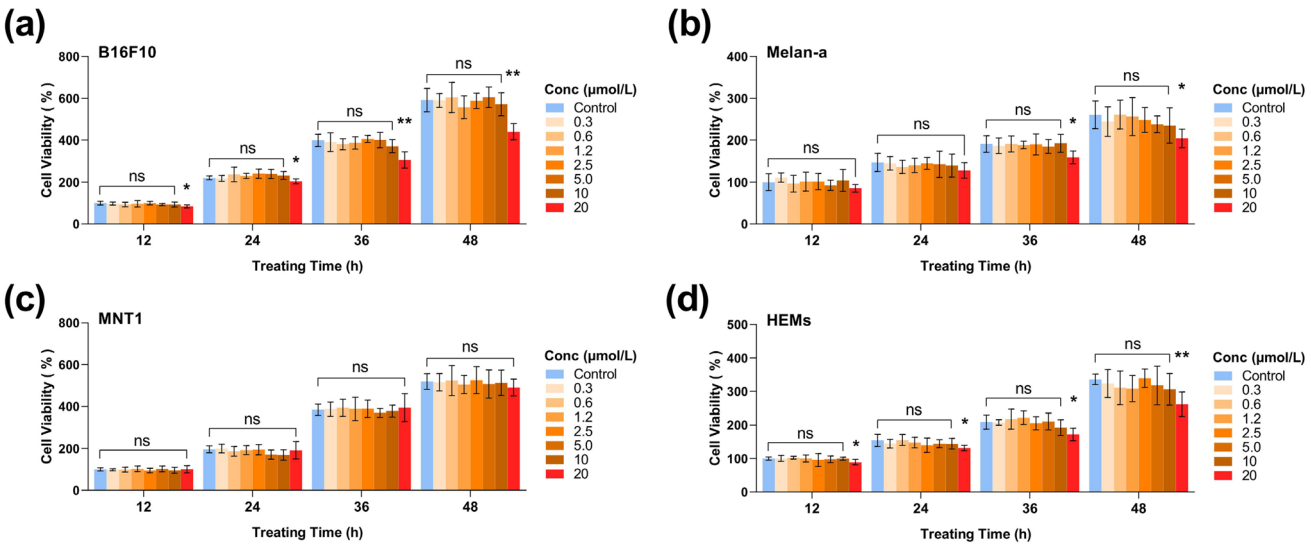

Fig. 2 Assay of RBFP cytotoxicity via MTT assay. Cells were treated with the resorufin-based fluorescence probe (RBFP) at different concentrations (0, 0.3, 0.6, 1.2, 2.5, 5.0, 10.0, and 20.0 μmol/L); absorption at 490 nm was measured with a microplate reader after 12, 24, 36, and 48 h of treatment; cell viability is expressed as a percentage: **a** B16F10; **b** Melan-a; **c** MNT1; **d** human epidermal melanocytes (HEMs) (data are presented as mean ± standard deviation, $n = 5$). Conc: concentration; ns: not significant; $^{*}P < 0.05$; $^{**}P < 0.01$

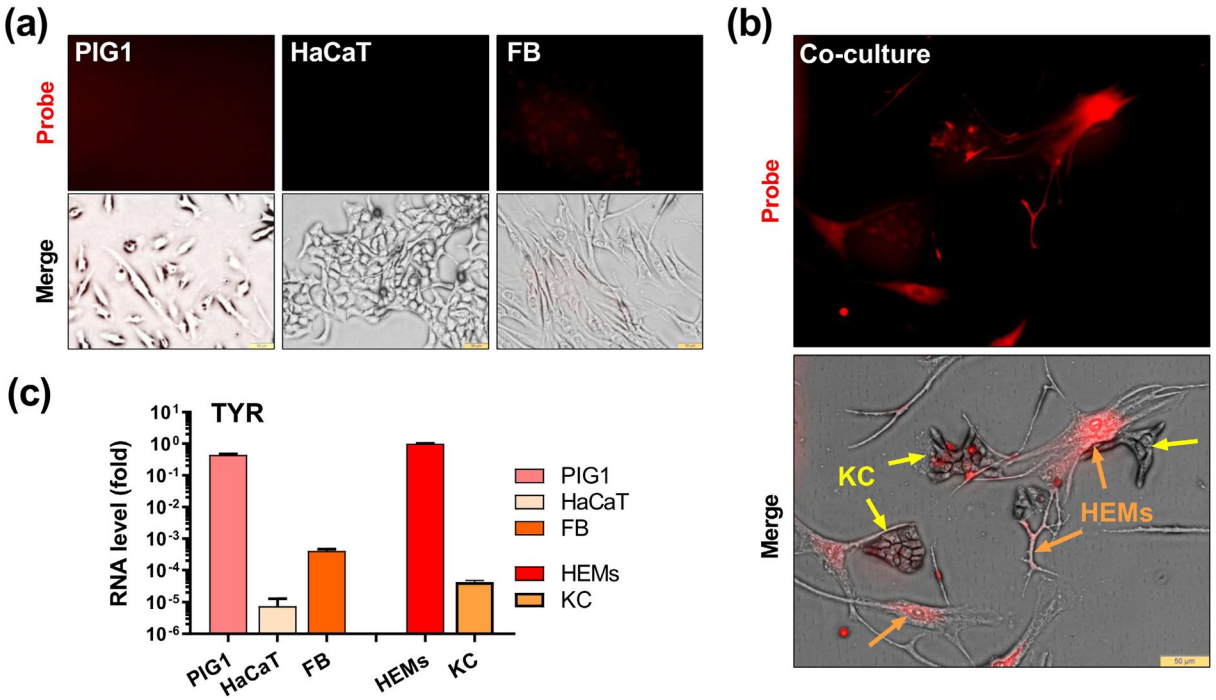

Fig. 3 The performance of the RBFP in different skin-cell types: **a** Fluorescence of PIG1, HaCaT, and fibroblasts (FB) after resorufin-based fluorescence probe (RBFP) treatment (5.0 μmol/L for 24 h); **b** Fluorescence of co-cultured human epidermal melanocytes (HEMs) and keratinocytes (KC) after RBFP treatment (5.0 μmol/L for 24 h), and orange arrows indicate HEMs and yellow arrows indicate KC; **c** RNA levels of tyrosinase (TYR) in different skin-cell types, determined by quantitative real-time reverse transcriptional polymerase chain reaction (qRT-PCR). Data are expressed as mean ± standard deviation ($n = 3$). Scale bar (light yellow) = 50 μm

in the 10 and 20 μmol/L groups at 48 h (Fig. 4b and 4c), due to residual catalyzed RBFP in the cells. However, fluorescence in MNT1 disappeared after 72 h (Fig. 4b).

Selectivity and sensitivity of the RBFP in cells

Results confirmed that the RBFP could detect TYR effectively in skin cells. Besides, our non-biological assessments showed that the RBFP had high selectivity and sensitivity for TYR. Based on that, we took a step further and used some biological tools for more evidence. First, we used mouse-specific siRNA to transfect B16F10 cells and downregulate TYR expression [29, 30]. Three siRNAs were designed for different targets on TYR messenger RNA (the sequences are given in Table S2). B16F10 cells were transfected with siRNAs (including a siRNA-a negative control) for 24 h, then treated with RBFP (5.0 μmol/L). Cell fluorescence was observed 24 h later. Fluorescence was markedly decreased in the si_TYR_3 group, but little changed in the other groups (Fig. 5a). qRT-PCR results showed that si_TYR_3 significantly decreased TYR RNA levels ($P < 0.01$) and that si_TYR_2 slightly decreased TYR RNA levels ($P < 0.05$), but si_TYR_1 had no effect (Fig. 5b). Second, we used kojic acid to suppress TYR activity in B16F10, Melan-a, MNT1, and HEMs, aiming to further confirm the selectivity and sensitivity of the RBFP. After 24 h, kojic acid-treated cells showed marked changes in cellular fluorescence, and intensity decreased gradually as kojic acid concentration increased (Fig. 5c–5f).

Performance of the RBFP in zebrafish

Zebrafish are widely used in melanin research and fluorescent imaging probe design [31], and PTU is commonly used in suppressing zebrafish TYR activity [32, 33]. Thus, we used zebrafish and PTU for in vivo studies. After hatching, zebrafish embryos were cultured with PTU (0.003%, equals to 200 μmol/L) to inhibit TYR and melanin formation [34]; the control group was treated with medium only. In the first two days, fluorescence was weak, with no noticeable difference between the two groups. However, on the fourth day, the NC group showed strong fluorescence, while the PTU-treated group continued to show weak fluorescence. After that, we removed the RBFP, thus fluorescence decreased markedly in all zebrafish on the fifth day. In addition, the density of melanin granules in the eyes, head, and tails of zebrafish gradually increased over time, except for the PTU-treated group (Fig. 6). In the first four days, the fluorescence intensity in the control group was closely related to melanin density.

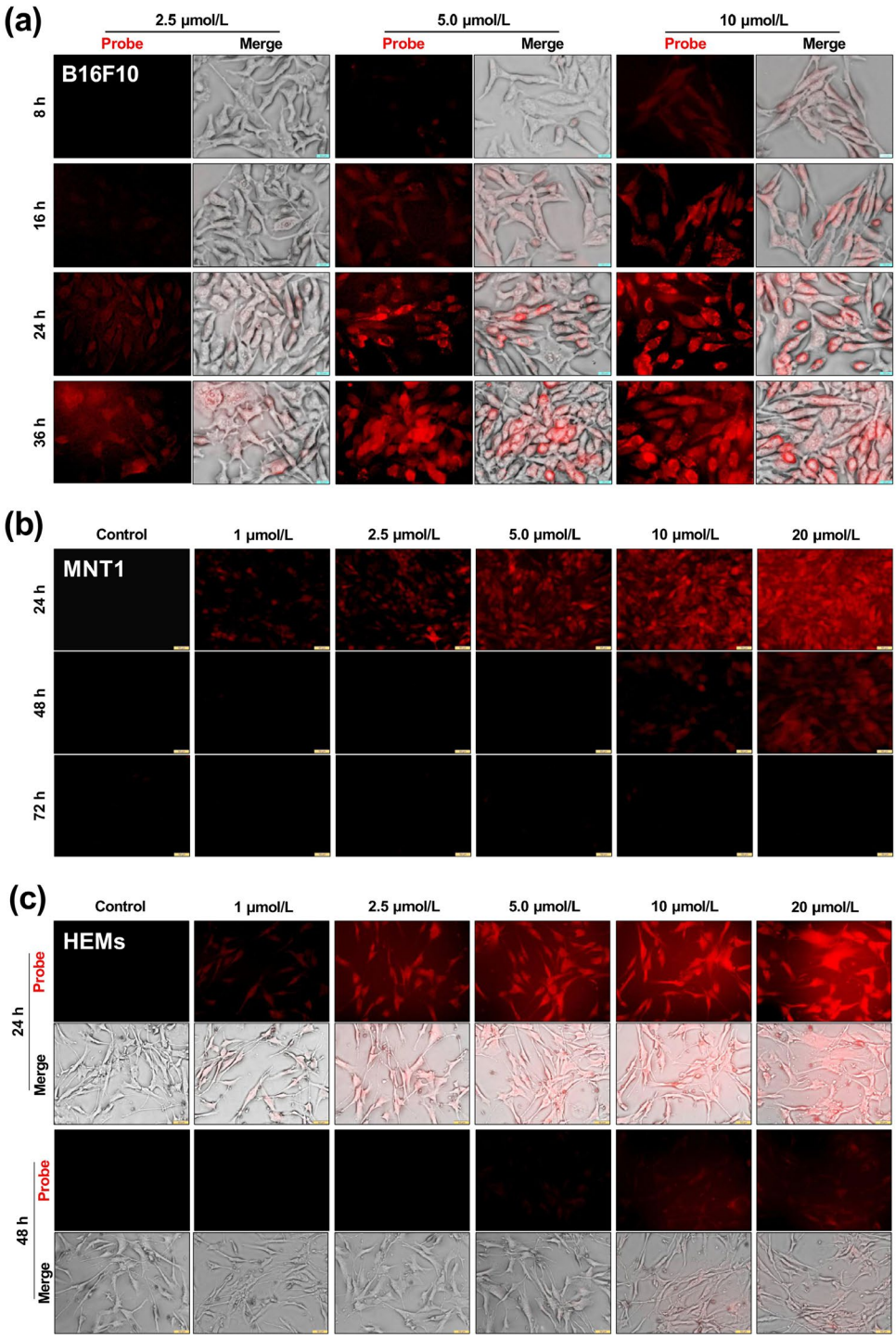

Fig. 4 Optimum observation conditions and clearance of the RBFP in cells. Cells were continuously treated with the RBFP at different concentrations (2.5, 5.0, and 10.0 μmol/L for B16F10; 1–20 μmol/L for MNT1 and HEMs). In B16F10, the RBFP was re-added after each observation to investigate the accumulation of probe in cells, but in MNT1 and HEMs, the RBFP was removed after 24 h to investigate the clearance of probe in cells. Fluorescence was observed at several time points (8, 16, 24, and 36 h in B16F10; and 24 and 36 h in MNT1 and HEMs): **a** B16F10; **b** MNT1; **c** HEMs. Scale bar (pale blue) = 20 μm and scale bar (light yellow) = 50 μm

Performance of the RBFP on guinea pig

To assess this probe in vivo, we used guinea pigs to evaluate the performance of RBFP in the skin. Different regions of the dorsal skin of guinea pigs were coated with kojic acid solution or PBS and then smeared with RBFP. On the second day, Region II (PBS + RBFP) showed strong red fluorescence, while Regions I (PBS), III (kojic acid), and IV (kojic acid + RBFP) were comparatively weak. These differences persisted, although less intensely, on the third day. After observation, the dorsal skin was washed to remove the RBFP residue and re-treated with kojic acid. On the fourth day, we found only weak fluorescence of RBFP-free skin, with no obvious differences between the four regions

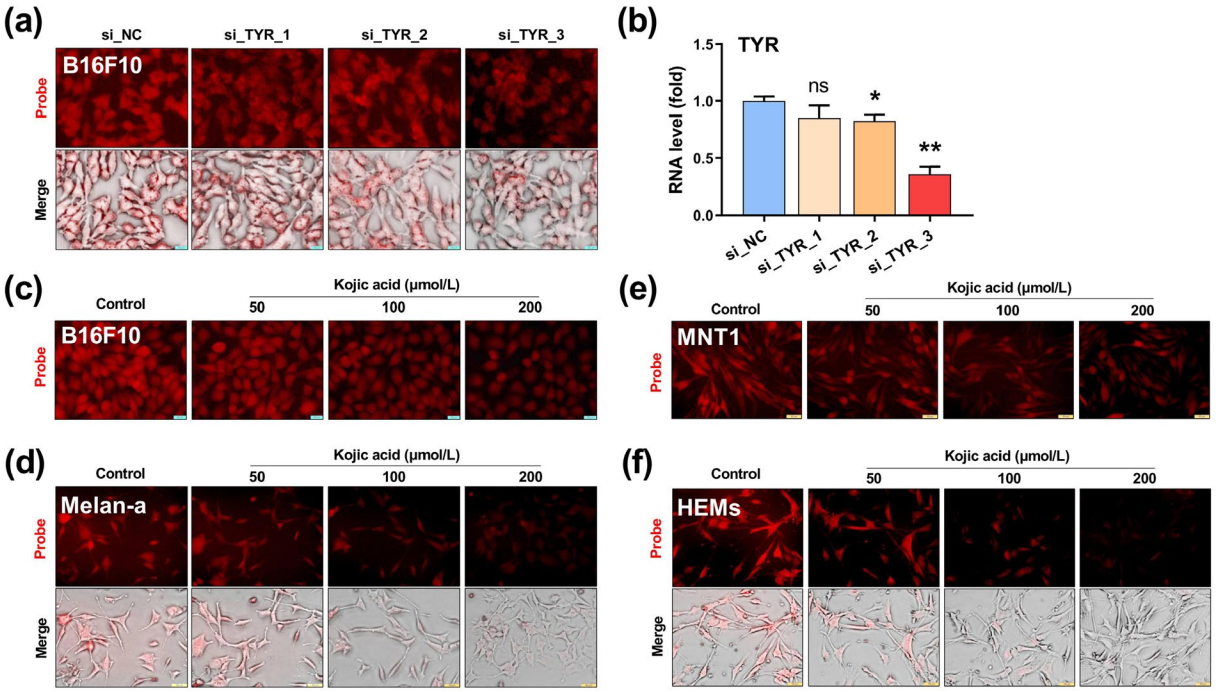

Fig. 5 Performance of the resorufin-based fluorescence probe (RBFP) after tyrosinase (TYR) expression or activity was suppressed by small interfering RNAs (siRNAs) or kojic acid. We transfected B16F10 cells with three different mouse TYR siRNAs or negative control (si_NC) for 48 h: **a** B16F10 cells were treated with the RBFP (5.0 μmol/L) at 24 h. and fluorescence was observed at 48 h. **b** RNA levels of TYR were measured by quantitative real-time reverse transcriptional polymerase chain reaction (qRT-PCR) (data are presented as the mean ± standard deviation, $n = 3$). Cells were also treated with kojic acid at several concentrations (50, 100, and 200 μmol/L) for 48 h. RBFP was added at 24 h and cellular fluorescence was observed 24 h later: **c** B16F10; **d** Melan-a; **e** MNT1; **f** HEMs. Scale bars (pale blue) = 20 μm and scale bars (light yellow) = 50 μm

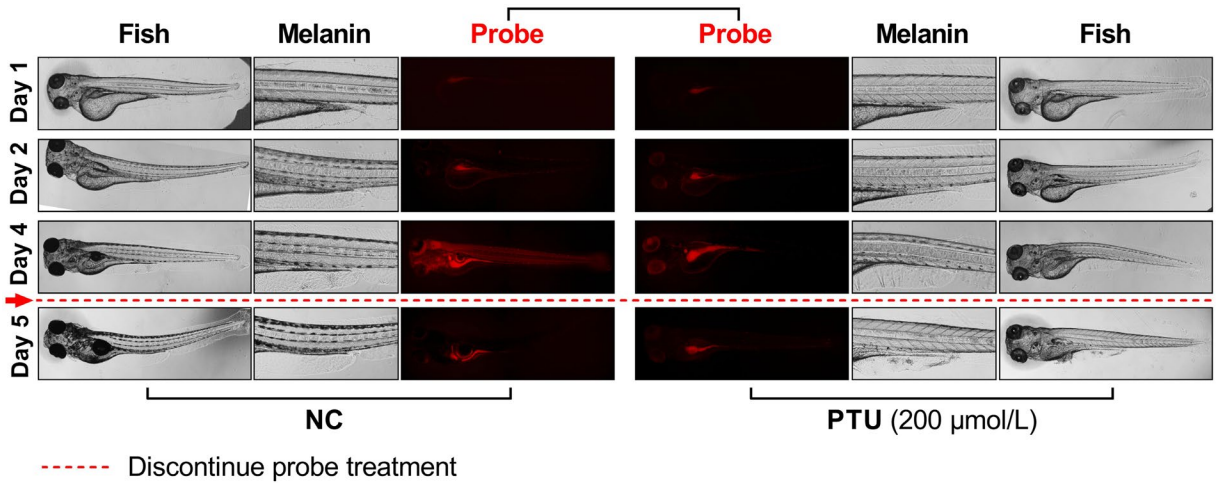

Fig. 6 Detection of tyrosinase (TYR) in zebrafish with the resorufin-based fluorescence probe (RBFP). After hatching, negative control group (NC) was cultured in medium, and others were treated with medium supplemented with 200 μmol/L 1-phenyl-2-thiourea (PTU). The RBFP (5.0 μmol/L) was added at baseline (day 0) and replaced with fresh probe after observed using fluorescence microscope, then the probe was removed after the observation on the fourth day

(Fig. 7a). After the experiment, we sampled dorsal skin from PBS-treated and PBS + RBFP-treated regions. No obvious skin erythema, papule, or scale was observed. We also found no histological differences between the skin from PBS-treated and PBS + RBFP-treated regions via HE staining. There was also no obvious inflammatory response (Fig. 7b).

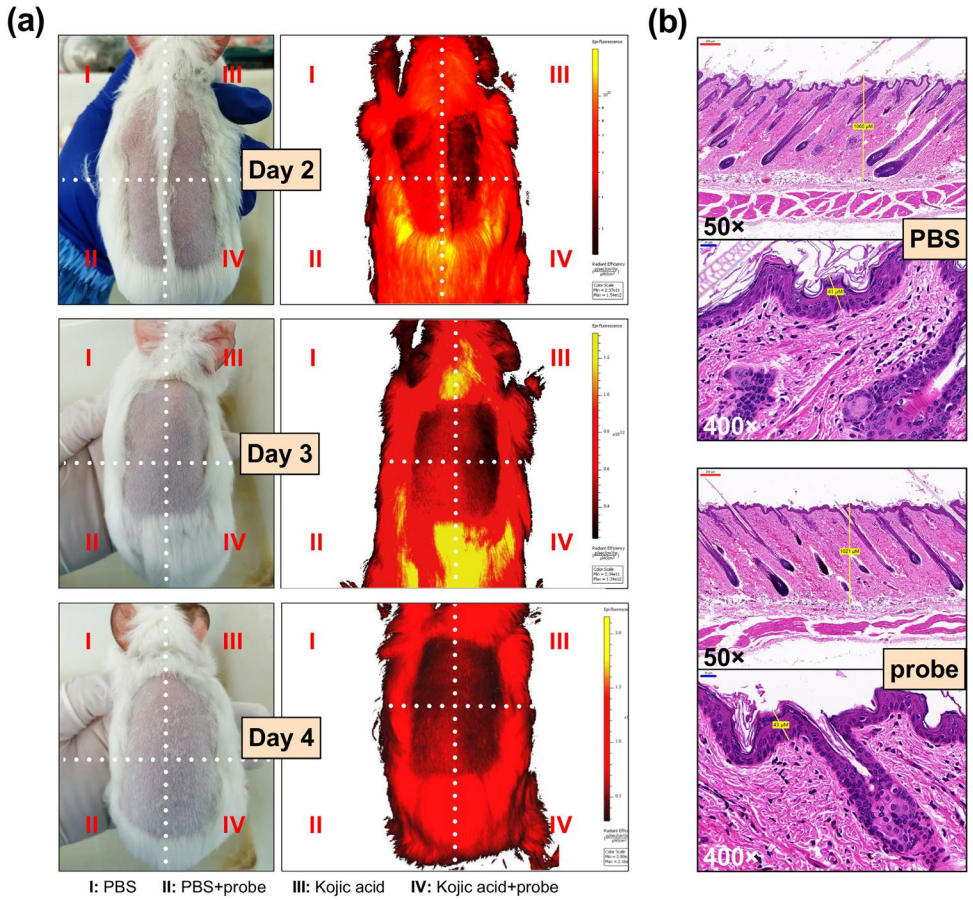

Fig. 7 Resorufin-based fluorescence probe (RBFP) performance on guinea pig skin. The dorsal skin of guinea pigs was shaved and divided into four regions, and each region was treated differently, as marked in the figures. Fluorescence was tested on the second, third, and fourth days after kojic acid (200 μmol/L) treatment; the RBFP (10 μmol/L) was added 4 h before observation: **a** an in vivo imaging system was used in fluorescence detection; **b** Hematoxylin–eosin (HE) staining showed the histology of dorsal skin collected from PBS-treated and PBS + RBFP-treated regions (50 × and 400 × views). Scale bar (red) = 200 μm and scale bar (blue) = 20 μm

Systemic toxicity assessment of the RBFP in vivo

To further evaluate probe toxicity, we coated the dorsal skin of SD rats with the RBFP (20 μmol/L). After a 3-d treatment, no skin abnormalities (including erythema, papule, and scale) were found in either the RBFP group or control group (Fig. 8a). Compared with the PBS group, HE staining showed that skin structure of rats was not affected by the RBFP (Fig. 8b), which was consistent with the impacts of RBFP on guinea pig skin (Fig. 7b). Further, the rats were euthanized and vital organs (including the heart, liver, spleen, lung, kidney, and stomach) were collected and examined. As shown in figures, no morphological changes of different organs were found after RBFP treatment. HE staining also showed no obvious pathological changes, such as inflammation and necrosis (Fig. 8c). The results confirm that the probe has no cutaneous or visceral toxicity.

Discussion

Preliminary in vitro experiments confirmed that this RBFP is potentially useful for quantitative determination of TYR levels. Our data demonstrate that the probe shows excellent selectivity and sensitivity for TYR in melanocytes and melanoma cells. The fluorescence is easy to detect across a wide range of time and concentrations. However, we still do not understand the exact mechanisms involved in RBFP uptake and clearance. Our studies indicate that 10 μmol/L RBFP is safe for both mouse and human cells, including B16F10, Melan-a, MNT1, and HEMs, and that catalyzed RBFP is cleared from cell cultures and whole animals (zebrafish) in a short time. The RBFP also shows no toxic effects when applied to the skin of guinea pigs and SD rats.

The epidermis contains both keratinocytes and melanocytes [35, 36], but only melanocytes can produce melanin. Thus, TYR expression in these two cell types was also significantly different. When we co-cultured HEMs and KCs together, the strong fluorescence in HEMs provided additional confirmation that this probe mainly works in melanocytes. Previous study has indicated that TYR in melanocytes can be secreted by vesicles or exosomes [37]. In our study, the fluorescence seen in some KC may be caused by melanosome-carried TYR from melanocytes. Moreover, unlike FB and HaCaT cells, PIG1 cells show only weak fluorescence, even though they have high TYR levels. However, the PIG1 cell line is extracted from Caucasian foreskin (generated by Le Poole IC, Seattle, USA) [38], and the TYR activity in

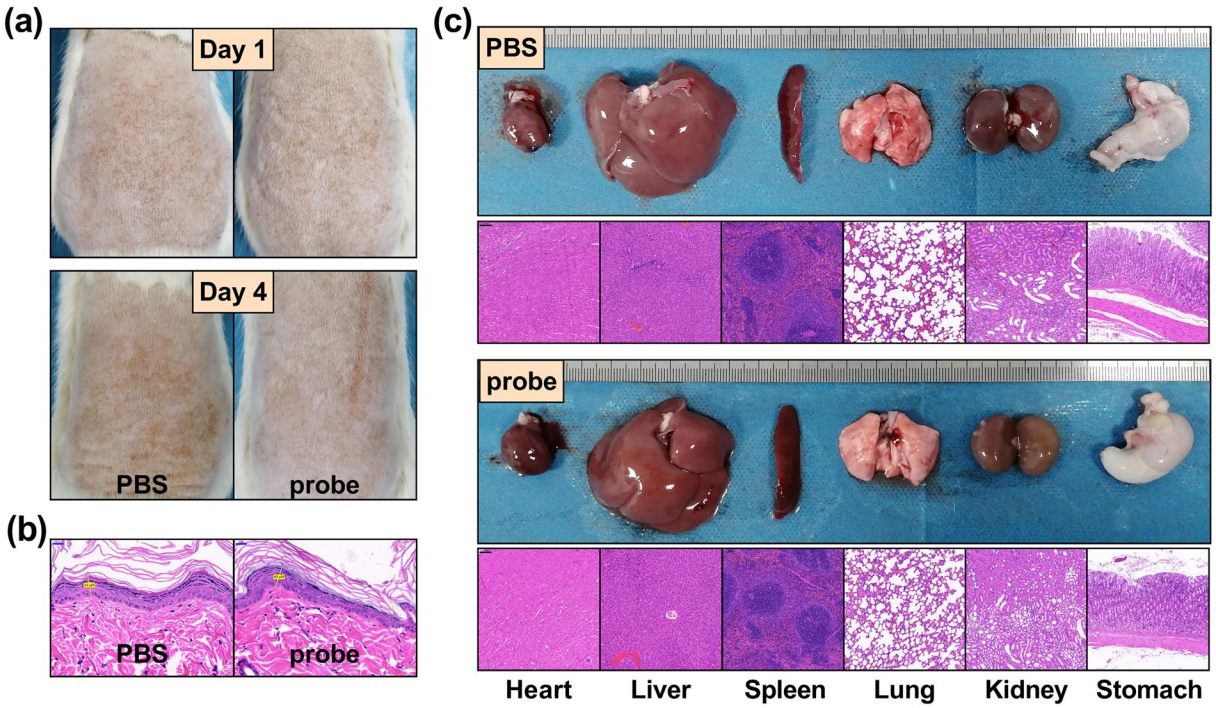

Fig. 8 Systemic toxicity assessment of the RBFP in SD rats. The dorsal skin of SD rats was shaved and treated with RBFP (20 μmol/L) for 3 d (applied twice a day). **a** The appearance of dorsal skin before and after treatment; **b** The histological view of dorsal skin from two groups (400 × magnification); **c** Morphology and histology of the heart, liver, spleen, lung, kidney, and stomach tissues (100 × magnification). Scale bar (blue) = 20 μm and scale bar (black) = 100 μm

Caucasian skin is relatively low. Overall, our findings indicate that this probe shows good selectivity for melanocytes and that selectivity may not be disturbed by the presence of other kinds of skin cells.

Abnormal TYR level is an important pathological feature of pigmentation disorders [20]. Several factors can regulate TYR messenger RNA (mRNA) levels or protein abundance [39]; it is of significance that this RBFP can detect the change of TYR levels when TYR is suppressed by siRNA transfection. Abnormal TYR activity is also an important feature of pigmentation disorders. TYR is an oxygen-dependent enzyme [40], while kojic acid is an effective inhibitor of TYR activation and is widely used in cosmetics and skin pigmentation disorder treatments [41, 42]. The probe can accurately reflect the changes in TYR activity caused by kojic acid treatment. Thus, the RBFP can respond to pigmentation disorders in two ways.

The probe also works in zebrafish and can be cleared in a short time. However, use of the RFBP in the zebrafish model has several limitations. We found strong fluorescence in the zebrafish belly, which may be caused by RBFP accumulation in the digestive tract [43]. In addition, fluorescence in zebrafish eyes disappeared in the control group, especially by the fifth day, indicating that RBFP fluorescence can be blocked by dense melanin granules. Moreover, zebrafish fluorescence was weak in the first few days of treatment, partly because the embryo was transported with PTU-supplied medium; and it took time for PTU to metabolize. These problems require additional evaluation of zebrafish models.

RBFP is also apparently effective on guinea pig skin. However, the red fluorescence of the RBFP on skin was seriously affected by endogenous fluorescence of guinea pig fur, including that of hair roots in the follicles. Although the human skin has less hair, the density of hair follicles is very high. Therefore, we suggest that the performance of this probe on skin should be evaluated more comprehensively, and our results so far do not definitively prove the clinical value of this probe in real skin. Unlike its performance in cells and zebrafish, the RBFP may encounter interference in practical use; given the interfering factors of dense melanin and hair, the probe needs further improved to address these issues.

Conclusions

This study evaluated the performance of a resorufin-based fluorescence probe (RBFP, synthesized by resorufin salt coupled with 3-(bromomethyl)phenol, first reported by Wu et al. [23–25]) in skin pigmentation disorders. Our work shows that the RBFP is safe, selective, and effective in melanocytes and melanocyte-derived cells. The fluorescence is

easily observed, and its intensity reflects the changes in TYR levels and activity in cells cultures. Additionally, the RBFP works well in zebrafish. However, the performance of the RBFP on guinea pig skin is not satisfactory; its limitations in this context have been discussed in the previous section.

In skin pigmentation disorders, abnormal TYR levels and activity are reliable indicators in diagnosis. Among skin cells, melanocytes are characterized by TYR levels. Thus, fluorescent TYR probes show clinical promise as diagnostic tools. One of the advantages of probes is that they are considered harmless and noninvasive when applied to the skin. Moreover, the fluorescence can be easily observed. However, the clinical usefulness of fluorescent probes on human skin remains to be verified, and its limitations in tests of animal models indicate the need for additional investigation. Melanocytes account for only a small proportion of skin components; therefore, it is essential that probes not be vulnerable to interference from other skin components, such as melanin and hair. Additionally, the effectiveness of transdermal delivery of probes and the intensity of the emitted fluorescence should be considered.

Supplementary Information The online version contains supplementary material available at https://doi.org/10.1007/s42242-021-00138-3.

Acknowledgements This work was supported by the National Natural Science Foundation of China (No. 82073420), the Project of Health and Family Planning Commission of Hunan Province (No. C2019173), the Wisdom Accumulation and Talent Cultivation Project of the Third Xiangya Hospital of Central South University (No. YX202007), the New Xiangya Talent Project of the Third Xiangya Hospital of Central South University (No. 20170301), and the Fundamental Research Funds for the Central Universities of Central South University (No. 2020zzts294), China.

Author contributions Conceptualization: JC, QHZ, HLZ; methodology: JC, SY; software & formal analysis: YBH, JXJ; validation: JHH, JC, QHZ; investigation: HLZ, YBH; data curation: YBH, QHZ, SY; writing-original draft: YBH, JC, JXJ; writing-review and editing: QHZ, JC; visualization: YBH; supervision: QHZ; project administration: JHH, QHZ, JC; funding acquisition: YBH, QHZ, JC. All authors have reviewed the last version of this manuscript and agreed to publish it.

Availability of data and materials The data that support the findings of this study are available from the corresponding author upon reasonable request.

Code availability Not applicable.

Declarations

Conflict of interest The authors declare that there is no conflict of interest.

Ethical approval All institutional and national guidelines for the care and use of laboratory animals were followed. Animal experiment protocols have been approved by the Animal Welfare Committee of the Department of Laboratory Animals, Central South University, Changsha, China.

Consent to participate Not applicable.

Consent for publication Not applicable.

References

1. Ezzedine K, Eleftheriadou V (2018) Vitiligo and quality of life: the dark face of whiteness. BJD 178(1):28–29. https://doi.org/10.1111/bjd.16072
2. Ezzedine K, Eleftheriadou V, Whitton M et al (2015) Vitiligo Lancet 386(9988):74–84. https://doi.org/10.1016/S0140-6736(14)60763-7
3. Ullah F, Schwartz RA, Edin F (2019) Nevus depigmentosus: review of a mark of distinction. Int J Dermatol 58(12):1366–1370. https://doi.org/10.1111/ijd.14393
4. Plensdorf S, Livieratos M, Dada N (2017) Pigmentation disorders: diagnosis and management. Am Fam Physician 96(12):797–804
5. Citek C, Herres-Pawlis S, Stack TD (2015) Low temperature syntheses and reactivity of Cu2O2 active-site models. Accounts Chem Res 48(8):2424–2433. https://doi.org/10.1021/acs.accounts.5b00220
6. Anello M, Fernandez E, Daverio MS et al (2019) TYR gene in llamas: polymorphisms and expression study in different color phenotypes. Front Genet 10:568. https://doi.org/10.3389/fgene.2019.00568
7. Oetting WS, King RA (1999) Molecular basis of albinism: mutations and polymorphisms of pigmentation genes associated with albinism. Hum Mutat 13(2):99–115. https://doi.org/10.1002/(SICI)1098-1004(1999)13:2%3c99::AID-HUMU2%3e3.0.CO;2-C
8. Cao J, Tyburczy ME, Moss J et al (2017) Tuberous sclerosis complex inactivation disrupts melanogenesis via mTORC1 activation. J Clin Invest 127(1):349–364. https://doi.org/10.1172/JCI84262
9. Speeckaert R, van Geel N (2017) Vitiligo: an update on pathophysiology and treatment options. Am J Clin Dermatol 18(6):733–744. https://doi.org/10.1007/s40257-017-0298-5
10. Jimbow K, Chen H, Park JS et al (2001) Increased sensitivity of melanocytes to oxidative stress and abnormal expression of tyrosinase-related protein in vitiligo. Brit J Dermatol 144(1):55–65. https://doi.org/10.1046/j.1365-2133.2001.03952.x
11. Ebanks JP, Wickett RR, Boissy RE (2009) Mechanisms regulating skin pigmentation: the rise and fall of complexion coloration. Int J Mol Sci 10(9):4066–4087. https://doi.org/10.3390/ijms10094066
12. Yun CY, Mi Ko S, Pyo Choi Y et al (2018) α-Viniferin improves facial hyperpigmentation via accelerating feedback termination of cAMP/PKA-signaled phosphorylation circuit in facultative melanogenesis. Theranostics 8(7):2031–2043. https://doi.org/10.7150/thno.24385
13. Zeng HJ, Liu Z, Hu GZ et al (2019) Investigation on the binding of aloe-emodin with tyrosinase by spectral analysis and molecular docking. Spectrochimica acta Part A, Spectrochim Acta A 211:79–85. https://doi.org/10.1016/j.saa.2018.11.045
14. Ezzedine K, Whitton M, Pinart M (2016) Interventions for vitiligo. JAMA 316(16):1708–1709. https://doi.org/10.1001/jama.2016.12399
15. Iannella G, Greco A, Didona D et al (2016) Vitiligo: pathogenesis, clinical variants and treatment approaches. Autoimmun Rev 15(4):335–343. https://doi.org/10.1016/j.autrev.2015.12.006

16. Passeron T, Picardo M (2018) Melasma, a photoaging disorder. Pigm Cell Melanoma R 31(4):461–465. https://doi.org/10.1111/pcmr.12684
17. Alghamdi KM, Kumar A, Taieb A et al (2012) Assessment methods for the evaluation of vitiligo. J Eur Acad Dermatol 26(12):1463–1471. https://doi.org/10.1111/j.1468-3083.2012.04505.x
18. Bae JM, Jung YS, Jung HM et al (2018) Classification of facial vitiligo: a cluster analysis of 473 patients. Pigm Cell Melanoma R 31(5):585–591. https://doi.org/10.1111/pcmr.12699
19. Farnetani F, Manfredini M, Chester J et al (2019) Reflectance confocal microscopy in the diagnosis of pigmented macules of the face: differential diagnosis and margin definition. Photoch Photobio Sci 18(5):963–969. https://doi.org/10.1039/c8pp00525g
20. Praetorius C, Sturm RA, Steingrimsson E (2014) Sun-induced freckling: ephelides and solar lentigines. Pigm Cell Melanoma R 27(3):339–350. https://doi.org/10.1111/pcmr.12232
21. Stromberg S, Bjorklund MG, Asplund A et al (2008) Transcriptional profiling of melanocytes from patients with vitiligo vulgaris. Pigm Cell Melanoma R 21(2):162–171. https://doi.org/10.1111/j.1755-148X.2007.00429.x
22. Tian Y, Zhang Z, Gao N et al (2020) A label-free luminescent assay for tyrosinase activity monitoring and inhibitor screening with responsive lanthanide coordination polymer nanoparticles. Spectrochim Acta B 228. https://doi.org/10.1016/j.saa.2019.117751
23. Wu X, Shi W, Li X et al (2019) Recognition moieties of small molecular fluorescent probes for bioimaging of enzymes. Acc Chem Res 52(7):1892–1904. https://doi.org/10.1021/acs.accounts.9b00214
24. Wu X, Li L, Shi W et al (2016) Near-infrared fluorescent probe with new recognition moiety for specific detection of tyrosinase activity: design, synthesis, and application in living cells and zebrafish. Angew Chem Int Edit 55(47):14728–14732. https://doi.org/10.1002/anie.201609895
25. Wu X, Li X, Li H et al (2017) A highly sensitive and selective fluorescence off-on probe for the detection of intracellular endogenous tyrosinase activity. Chem Commun 53(16):2443–2446. https://doi.org/10.1039/c6cc09679d
26. Pei S, Chen J, Lu J et al (2019) The long noncoding RNA UCA1 negatively regulates melanogenesis in melanocytes. J Invest Dermatol 140(1):152–163. https://doi.org/10.1016/j.jid.2019.04.029
27. Fu T, Chai B, Shi Y et al (2019) Fargesin inhibits melanin synthesis in murine malignant and immortalized melanocytes by regulating PKA/CREB and P38/MAPK signaling pathways. J Dermatol Sci 94(1):213–219. https://doi.org/10.1016/j.jdermsci.2019.03.004
28. Kang M, Park SH, Park SJ et al (2019) p44/42 MAPK signaling is a prime target activated by phenylethyl resorcinol in its antimelanogenic action. Phytomedicine 58. https://doi.org/10.1016/j.phymed.2019.152877
29. Castel SE, Martienssen RA (2013) RNA interference in the nucleus: roles for small RNAs in transcription, epigenetics and beyond. Nat Rev Genet 14(2):100–112. https://doi.org/10.1038/nrg3355
30. Hannon GJ, Rossi JJ (2004) Unlocking the potential of the human genome with RNA interference. Nature 431(7006):371–378. https://doi.org/10.1038/nature02870
31. Motiani RK, Tanwar J, Raja DA, et al. (2018) STIM1 activation of adenylyl cyclase 6 connects Ca^{2+} and cAMP signaling during melanogenesis. EMBO J 37:e97597. https://doi.org/10.15252/embj.201797597
32. MacDonald TC, Nehzati S, Sylvain NJ et al (2015) Phenylthiourea alters toxicity of mercury compounds in zebrafish larvae. J Inorg Biochem 151:10–17. https://doi.org/10.1016/j.jinorgbio.2015.07.003
33. Favre E, Daina A, Carrupt PA et al (2014) Modeling the met form of human tyrosinase: a refined and hydrated pocket for antagonist design. Chem Biol Drug Des 84(2):206–215. https://doi.org/10.1111/cbdd.12306
34. Bohnsack BL, Gallina D, Kahana A (2011) Phenothiourea sensitizes zebrafish cranial neural crest and extraocular muscle development to changes in retinoic acid and IGF signaling. PLoS ONE 6(8). https://doi.org/10.1371/journal.pone.0022991
35. Calleja-Agius J, Brincat M, Borg M (2013) Skin connective tissue and ageing. Best Pract Res Cl Ob 27(5):727–740. https://doi.org/10.1016/j.bpobgyn.2013.06.004
36. Rippa AL, Kalabusheva EP, Vorotelyak EA (2019) Regeneration of dermis: scarring and cells involved. Cells 8(6):607. https://doi.org/10.3390/cells8060607
37. Cullinane AR, Vilboux T, O'Brien K et al (2011) Homozygosity mapping and whole-exome sequencing to detect SLC45A2 and G6PC3 mutations in a single patient with oculocutaneous albinism and neutropenia. J Invest Dermatol 131(10):2017–2025. https://doi.org/10.1038/jid.2011.157
38. le Poole IC, van den Berg FM, van den Wijngaard RM et al (1997) Generation of a human melanocyte cell line by introduction of HPV16 E6 and E7 genes. Vitro Cell Dev Biol - Animal 33:42–49. https://doi.org/10.1007/s11626-997-0021-6
39. Mortimer SA, Kidwell MA, Doudna JA (2014) Insights into RNA structure and function from genome-wide studies. Nat Rev Genet 15(7):469–479. https://doi.org/10.1038/nrg3681
40. Washington C, Maxwell J, Stevenson J et al (2015) Mechanistic studies of the tyrosinase-catalyzed oxidative cyclocondensation of 2-aminophenol to 2-aminophenoxazin-3-one. Arch Biochem Biophys 577–578:24–34. https://doi.org/10.1016/j.abb.2015.04.007
41. Cabanes J, Chazarra S, Garcia-Carmona F (1994) Kojic acid, a cosmetic skin whitening agent, is a slow-binding inhibitor of catecholase activity of tyrosinase. J Pharm Pharmacol 46(12):982–985. https://doi.org/10.1111/j.2042-7158.1994.tb03253.x
42. Saeedi M, Eslamifar M, Khezri K (2019) Kojic acid applications in cosmetic and pharmaceutical preparations. Biomed Pharmacother 110:582–593. https://doi.org/10.1016/j.biopha.2018.12.006
43. Ji J, Merino S, Tomas JM et al (2019) Nanoliposomes encapsulating immunostimulants modulate the innate immune system and elicit protection in zebrafish larvae. Fish Shellfish Immun 92:421–429. https://doi.org/10.1016/j.fsi.2019.06.016